TISSUE ENGINEERING: Part A
Volume 20, Numbers 23 and 24, 2014

DOI: 10.1089/ten.tea.2013.0663

Total Body Irradiation Is Permissive for Mesenchymal Stem Cell-Mediated New Bone Formation Following Local Transplantation

Samuel Herberg, PhD,[1,2] Galina Kondrikova, BS,[1,2] Khaled A. Hussein, PhD,[3] Sudharsan Periyasamy-Thandavan, PhD,[1,2] Maribeth H. Johnson, MS,[4] Mohammed E. Elsalanty, MD, PhD,[3,5] Xingming Shi, PhD,[5–7] Mark W. Hamrick, PhD,[2,5,7] Carlos M. Isales, MD,[2,5–7] and William D. Hill, PhD[1,2,5,7]

Skeletal injury is a major clinical challenge accentuated by the decrease of bone marrow-derived mesenchymal stem/stromal cells (BMSCs) with age or disease. Numerous experimental and clinical studies have revealed that BMSCs hold great promise for regenerative therapies due to their direct osteogenic potential and indirect trophic/paracrine actions. Increasing evidence suggests that stromal cell-derived factor-1 (SDF-1) is involved in modulating the host response to the injury. Common problems with BMSC therapy include poor cell engraftment, which can be addressed by total body irradiation (TBI) prior to transplantation. In this study, we tested the hypothesis that direct tibial transplantation of BMSCs drives endogenous bone formation in a dose-dependent manner, which is enhanced by TBI, and investigated the potential role of SDF-1 in facilitating these events. We found that TBI is permissive for transplanted BMSCs to engraft and contribute to new bone formation. Bone marrow (BM) interstitial fluid analysis revealed no differences of SDF-1 splice variants in irradiated animals compared to controls, despite the increased mRNA and protein levels expressed in whole BM cells. This correlated with increased dipeptidyl peptidase IV activity and the failure to induce chemotaxis of BMSCs *in vitro*. We found increased mRNA expression levels of the major SDF-1-cleaving proteases in whole BM cells from irradiated animals suggesting distinct spatial differences within the BM in which SDF-1 may play different autocrine and paracrine signaling roles beyond the immediate cell surface microenvironment.

Introduction

Skeletal injuries, including osteoporotic fractures, and their complications continue to be major causes of morbidity and mortality.[1] These clinical challenges are accentuated by the decrease in the number of bone marrow-derived mesenchymal stem/stromal cells (BMSCs) with age or disease.[2] The loss of BMSCs may be due to increased cell death, reduced proliferation, mobilization from and recirculation to the bone marrow (BM) niche, or a change in the rate of differentiation along the adipogenic lineage rather than the osteogenic lineage.[3,4]

Over the last decade, numerous studies have revealed that BMSCs hold great potential for cell-based therapy due to their multilineage potential.[5] Both autologous and allogeneic BMSCs have been utilized to repair or regenerate bone in experimental and clinical studies.[6,7] However, the translation of these pilot trials into routine clinical practice faces many challenges with regard to the *ex vivo* culture conditions of BMSCs, specifically the gradual loss of potency and possible acquisition of replicative senescence.[8] Another difficulty with BMSC therapy is that cells almost universally fail to significantly engraft within the BM when infused into the peripheral circulation of animal and human subjects.[9–11] Systemic infusion of BMSCs does not promote an osteogenic response in bone due to both the ''pulmonary first-pass effect'' causing more than 96% of cells to become entrapped in the lung microvasculature and the poor long-term engraftment

This work was performed at the Augusta Veterans Affairs Medical Center and Georgia Regents University.
[1]Charlie Norwood VA Medical Center, Georgia Regents University, Augusta, Georgia.
Departments of [2]Cellular Biology and Anatomy, [3]Oral Biology, and [4]Biostatistics and Epidemiology, Georgia Regents University, Augusta, Georgia.
[5]Institute for Regenerative and Reparative Medicine, Georgia Regents University, Augusta, Georgia.
Departments of [6]Neuroscience and Regenerative Medicine and [7]Orthopaedic Surgery, Georgia Regents University, Augusta, Georgia.

beyond 4–8 weeks.[12,13] After being transplanted, BMSCs can face a complex adverse environment featuring inflammatory reactions, hypoxia, and oxidative stress, which can promote cell death.[14] Furthermore, mobilized or cultured BMSCs may not express the appropriate cell surface receptors or have access to engraftment sites in the BM niche without modification. A common approach to address these issues is irradiation preconditioning. Total body irradiation (TBI) efficiently ablates host stem cell populations and has been shown to enhance cell engraftment during subsequent transplantation of whole BM or BMSCs.[15–18] In allogeneic transplantation, irradiation also prevents the host immune response toward the graft.[19]

Recently, it has been postulated that indirect actions of implanted BMSCs, such as the release of paracrine factors in the microenvironment modulating the host response to injury, are as important in bone tissue regeneration as their direct ability to form new bone.[20–22] The knowledge of the trophic actions of BMSCs and their temporal sequence during fracture repair, in particular, may lead to novel therapeutic approaches in the treatment of nonunions.[8] Among the molecules exerting paracrine effects is stromal cell-derived factor-1 (SDF-1)/CXCL12, a member of the pro-inflammatory CXC chemokine family.[23] SDF-1 and its main G-protein-coupled CXC chemokine receptor 4 (CXCR4) are expressed constitutively in various tissues.[24–26] Binding of SDF-1 to CXCR4 initiates diverse downstream signaling processes,[27] including the recruitment of regenerative cells to injury sites during the acute phase of bone repair.[13,28,29] Compelling evidence suggests that regulated proteolytic degradation plays a critical role in the control of SDF-1 function.[30–36]

The objective of this study was to investigate cell engraftment of recently described BMSCs[14,37] and new bone formation upon administration of a single lethal dose of TBI in skeletally mature C57BL/6J male mice, and the potential role of the chemokine SDF-1 in facilitating these events in the BM microenvironment. We tested the hypothesis that direct intramedullary tibial transplantation of BMSCs drives endogenous bone formation in a dose-dependent manner, which is enhanced by irradiation preconditioning.

Materials and Methods

Animals

C57BL/6J male mice were purchased from Jackson Laboratories. Animals were maintained at the Laboratory Animal Services research facility at Georgia Regents University and used at the age of 6 months. All aspects of the research were conducted in accordance with the guidelines set by the Georgia Regents University Institutional Animal Care and Use Committee following an approved Animal Use Protocol (protocol number 2011-0397).

Isolation and culture of BMSCs

Six 18-month-old male C57BL/6J mice, purchased from the National Institute on Aging aged rodent colony, were used to obtain BMSCs at the Georgia Regents University Stem Cell Core Facility as described previously.[14,37–39] First, mice were euthanized by CO_2 overdose followed by thoracotomy. The femora and tibiae were dissected free of soft tissues and kept in cold phosphate-buffered saline (PBS) on ice. The bones were cut open at both ends and flushed with complete isolation media (CIM) (RPMI-1640; Cellgro, Mediatech), 9% heat-inactivated fetal bovine serum (FBS), 9% horse serum (both from Atlanta Biologicals), and 12 μM L-glutamine (Gibco, Invitrogen) using a 22-gauge syringe followed by filtration through a 70-μm nylon mesh filter. The combined whole BM aspirate was dispersed with a 25-gauge syringe to produce a single cell suspension. Next, BMSCs were isolated using a modified protocol[40–42] by plating the single cell suspension in 175-cm^2 flasks at a density of 2×10^7 cells/flask. After 3-h incubation at 37°C in 5% CO_2, the nonadherent cells were removed and the adherent cells gently washed twice with PBS to reduce the degree of hematopoietic lineage cell contamination. The cells were cultured in CIM for 3–4 weeks with media change every 3–4 days. At 70–80% confluence, the cells were lifted with trypsin/ethylenediaminetetraacetic acid (EDTA), washed, and resuspended at a density of 5×10^6 cells/mL in PBS containing 0.5% bovine serum albumin (BSA) and 2 mM EDTA followed by negative immunodepletion using magnetic microbeads conjugated to anti-mouse CD11b, CD45R/B220 (BD Biosciences Pharmingen), CD11c, and PDCA-1 (Miltenyi Biotec) monoclonal antibodies according to the manufacturer's instructions. Resulting CD11b, CD45R/B220, CD11c, PDCA-1-negative cells were subjected to positive immunoselection using anti-Sca-1 microbeads (Miltenyi Biotec) following the manufacturer's recommendations. Enriched BMSCs (0.33% CD45, 0.13% CD11b, and 83.18% Sca-1 by FACS analysis[38]), which are depleted of monocytes, granulocytes, macrophages, myeloid-derived dendritic cells (DCs), natural killer cells, B-1 cells, B lymphocytes, T lymphocytes, classical DCs, plasmacytoid DCs, and macrophage progenitors, were maintained in Dulbecco's modified Eagle's medium (DMEM; Cellgro) with 10% heat-inactivated FBS (Atlanta Biologicals), and shown of possessing multilineage potential.[38] BMSCs were subjected to retroviral-mediated transduction with ΔU3-GFP plasmid DNA, constructed in the replication defective ΔU3nlsLacZ vector by inserting the full-length coding region of *Gfp* cDNA.[39] BMSCs were seeded at low density for clonal selection. Well-isolated, GFP-positive BMSCs (clone 2) were maintained in DMEM supplemented with 10% heat-inactivated FBS and used at 70–80% confluence.

Total body irradiation

Irradiation doses of 7.0–13.0 Gy have been shown to be myeloablative.[43–45] Higher doses can cause the animals to die secondary to irradiation-induced toxicity while lower doses may prolong the time necessary to achieve sufficient donor engraftment.[44] Fifty-six 6-month-old C57BL/6 male mice were divided into two groups. Twenty-eight recipient mice received a lethal dose (8.25 Gy) of TBI at 0.825 Gy/min for 10 min using a cesium-137 source (Gammacell 40 Exactor; Best Theratronics) without shielding, as previously described,[46] since this dose has been shown to result in 0% survival after 30 days in untreated mice.[47] Twenty-eight nonirradiated animals were used as controls. The next day, lethally irradiated mice were anesthetized with 2% isoflourane and transplanted with 6.0×10^6 cells/mL of rescuing whole BM, obtained from femora and tibiae of donor

litter mates, supplemented with 1% diprotin A to enhance BM cell engraftment[46,48] (Peptide Institute) by injection into the retro-orbital sinus (Supplementary Fig. S1; Supplementary Data are available online at www.liebertpub.com/tea).

Intramedullary tibial transplantation

Direct intramedullary tibial transplantations were performed according to a modified protocol.[16,46] First, lethally irradiated and control recipient mice were anesthetized with 2% isoflourane followed by subcutaneous injection of 2.5 mg/kg carprofen for presurgical analgesia. The injection site was shaved and 10% betadine solution (Purdue Products L.P.) applied topically. The knee was flexed to 90° and the proximal end of the tibia drawn to the anterior. A 26-gauge needle was inserted into the joint surface of the tibia through the patellar tendon and then inserted into the medullary space. The needle was removed; a second 26-gauge needle inserted into the needle track and extended into the BM space to flush with 100 µL 0.9% saline. BMSCs[14,37] at 1.32×10^5 (1% dose), 1.32×10^6 (10% dose), 6.60×10^6 (50% dose), or 1.32×10^7 cells/mL (100% dose), supplemented with 1% diprotin A to enhance BMSC engraftment[48] (Peptide Institute) were slowly injected into the left marrow cavity as the needle was withdrawn from the intramedullary space (70 µL; 9.24×10^3, 9.24×10^4, 4.62×10^5, 9.24×10^5 cells total; $n=7$/group). Right tibiae were injected with vehicle control (Supplementary Fig. S1). Recipient mice were fed with regular animal chow and had access to antibiotic-containing water (Hi-Tech Pharmacal) for 2 days before switching to water *ad libitum*. After 4 weeks, animals were euthanized by subcutaneous administration of a ketamine HCl (85 mg/kg; IP)/xylazine HCl (15 mg/kg; IP) cocktail followed by thoracotomy. Tibiae were removed, dissected free of soft tissues, and fixed in 3% paraformaldehyde. After 24 h, specimens were washed in PBS and preserved in 70% ethyl alcohol at 4°C.

Isolation of whole BM cells and BM interstitial fluids

Whole BM cells and BM interstitial fluids were isolated from femora and humeri as described previously.[37] The femora and tibiae were dissected free of soft tissues and kept on ice. A 15-mL conical tube was filled with 1 mL of PBS prior to cutting the bones into small pieces to release their BM cells. Following vigorous mixing, the BM cell suspensions were separated from the bone chips using a 100-µL pipette and divided in two 500-µL aliquots. BM cells were subsequently pelleted at 1500 rpm for 5 min and samples were transferred to −80°C for later use.

Microcomputed tomography

Tibiae were scanned with an *ex vivo* microcomputed tomography (µCT) system (Skyscan 1174; Skyscan). The scanner was equipped with a 50 kV, 800 µA X-ray tube and a 1.3 megapixel CCD coupled to a scintillator. Four tibiae were placed in a plastic sample holder with the long axes oriented parallel to the image plane and scanned in air using 15-µm isotropic voxels, 400 ms integration time, 0.5° rotation step, 360° rotation, and frame averaging of 5. All samples were scanned within the same container using the same scanning parameters. All scans were then reconstructed using NRecon software v1.6.6.0 (Skyscan) with exactly the same reconstruction parameters (window width: 0–255 [grayscale)]/0–0.1204 [attenuation coefficient]; window level: 128 [grayscale]/0.0602 [attenuation coefficient]). For three-dimensional (3D) analysis (CTAn software v1.12.0.0+, Skyscan), the grayscale was set from 60 to 140. This range allowed viewing of the normal bone architecture seen in the raw images. All reconstructed images were adjusted to this grayscale before running the 3D analysis. Standard 3D morphometric parameters[49] were determined in a region of interest (ROI) starting immediately beyond the epiphyseal plate (transaxial tracing; 135 cuts = 2 mm distally; Fig. 1) in all samples. For bone mineral density (BMD [trabecular bone]) measurements using the same ROI, calibration was performed with 0.25 and 0.75 mg/cc

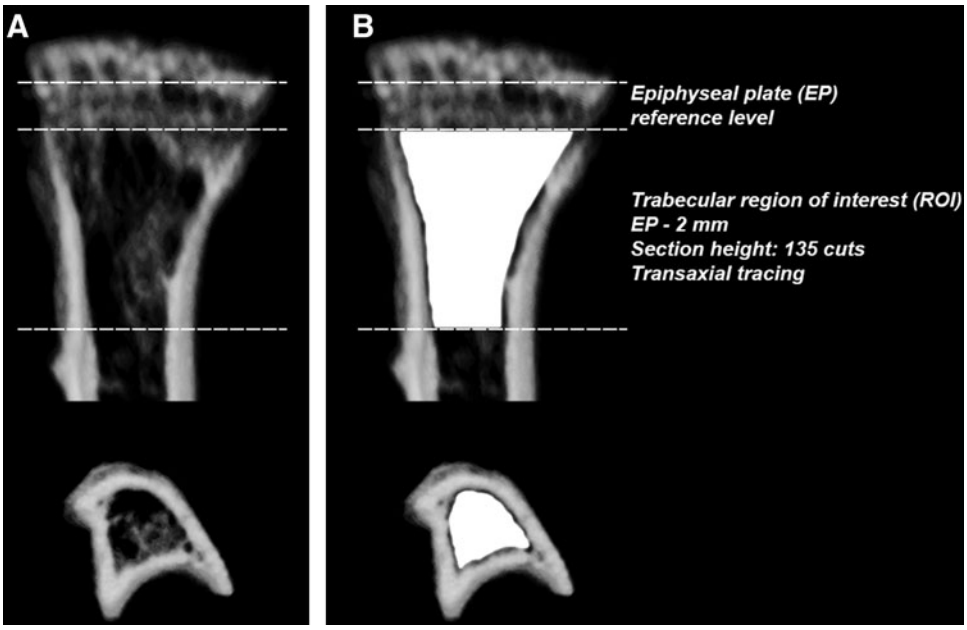

FIG. 1. Schematic of the trabecular region of interest (ROI) for three-dimensional (3D) bone morphometric analysis using microcomputed tomography (µCT). **(A)** Transverse and coronal views of a representative proximal tibia. **(B)** Using the epiphyseal plate (EP) as a reference level, quantitative analyses of trabecular bone morphometric parameters were performed using an ROI (delineated by the Skyscan CTAn software tool using freehand drawing depicted in white) starting immediately beyond the EP and extending 135 cuts/2-mm distally by transaxial tracing.

hydroxyapatite phantoms (Skyscan) as per the manufacturer's protocol. Representative 3D images were created using CTvox software v2.3.0 r810 (Skyscan).

Histological preparation and analysis

Tibiae were decalcified in 0.25 M EDTA at pH 7.4 for 7 days at 4°C with changes of the EDTA solution every other day. Specimens were washed, dehydrated in a graded series of ethyl alcohol (70–100%), cleared in xylene, embedded longitudinally in paraffin, and sectioned at 5-μm thickness using a microtome (Leica Microsystems, Inc.) prior to mounting on Frost Plus glass slides for histology. Serial sections were stained with standard hematoxylin and eosin (H&E) for histologic analysis. Light microscopy images were captured using a Carl Zeiss microscope (Carl Zeiss, Inc.) with AxioVision Image Analysis software v4.7.1.0.

Bone histomorphometry

The standard two-dimensional (2D) histomorphometric parameter[50,51] percent bone volume (BV/TV) was assessed in the proximal tibiae ($n=3$ animals per group) employing a 876.9×657.1 μm rectangular ROI (H&E-stained central sections, 20×, 1388×1040 pixels per image, 576211.68 μm^2 or 0.58 mm^2 combined total area in four identical quadrants; Fig. 2A) according to an established protocol.[52] First, black-and-white image masks of the H&E-stained color images were created using the wand tool (tolerance: 10) in Photoshop CS6 software v13.0 (Adobe Systems) to highlight areas of bone. In all 20× images, bone tissue was designated in black while the remaining tissue was designated in white, creating the mask for analysis (Fig. 2B–D). Next, using ImageJ software 1.47v (NIH), the entire image area was calculated as tissue area (T.Ar) and, using the default wand tool, the combined black-colored areas were summarized as bone area (B.Ar) to calculate percent bone volume (BV/TV). Per definition, BV/TV is numerically identical with the corresponding area/area ratio B.Ar/T.Ar.[50]

Immunohistochemistry

Five micrometer paraffin sections were deparaffinized in xylene, hydrated, and permeabilized in 0.1% Triton X-100 for 10 min. Antigen retrieval was performed using the Digest-All-3 solution (Invitrogen). Nonspecific binding was blocked using 3% normal donkey serum or 3% normal goat serum (Jackson ImmunoResearch) for 1 h at room temperature in a humidifying chamber. Serial sections were incubated with a primary antibody overnight at 4°C (Table 1). For detection of immunopositive signals, sections were

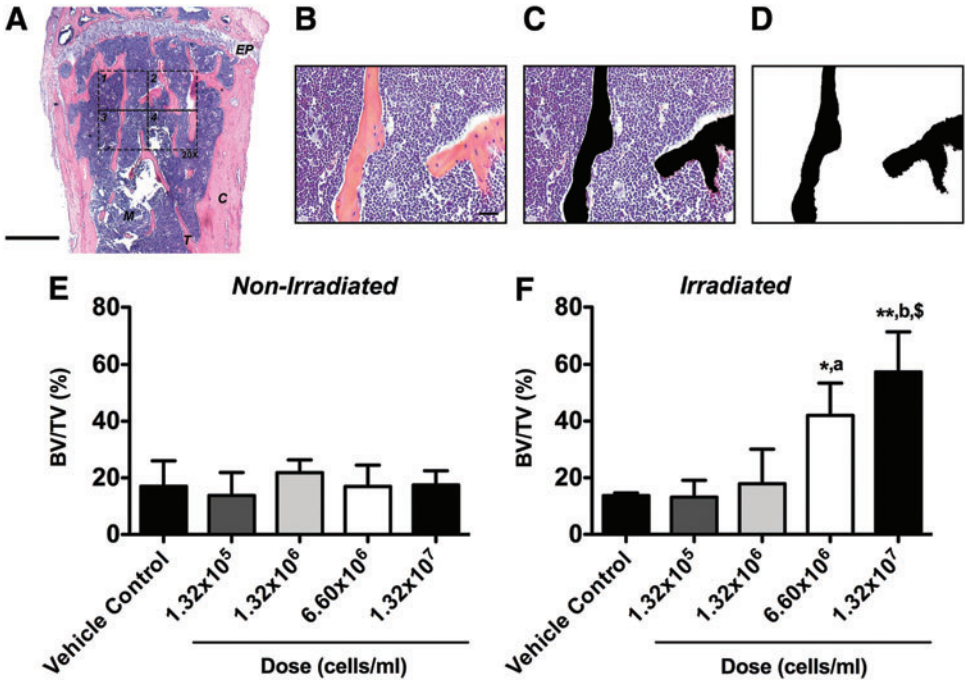

FIG. 2. Total body irradiation (TBI) significantly increases two-dimensional (2D) bone volume following BMSC transplantation in a cell dose-dependent fashion. The standard 2D bone histomorphometric parameter BV/TV was assessed in the proximal tibiae 4 weeks post-transplantation. **(A)** Overview of a representative hematoxylin and eosin (H&E)-stained central cross-section (EP: epiphyseal plate, M: marrow, T: trabecular bone, C: cortical bone, 2.5×, scale bar 500 μm). The 876.9×657.1 μm rectangular ROI (20×, scale bar 20 μm, 1388×1040 pixels per image, 576211.68 μm^2 or 0.58 mm^2 combined total area in four identical quadrants) is outlined in dashed lines. **(B)** One H&E-stained central cross-section 20× ROI quadrant. **(C)** The same 20× ROI depicting bone tissue in black (Photoshop wand tool, tolerance: 10). **(D)** Final black-and-white image mask of the 20× ROI showing bone tissue in black and all other tissue in white. Using ImageJ, the entire image area was calculated as tissue area (T.Ar) and the black-colored area was summarized as bone area (B.Ar; default ImageJ wand tool) to calculate BV/TV. Per definition, BV/TV is numerically identical with the corresponding area/area ratio B.Ar/T.Ar. **(E)** Nonirradiated and **(F)** irradiated animals (*$p<0.05$, **$p<0.01$ BMSC-transplanted vs. vehicle controls; $^{a}p<0.05$, $^{b}p<0.01$ 1.32×10^5 cells/mL vs. higher doses; $^{\$}p<0.01$ 1.32×10^6 cells/mL vs. higher doses, $n=3$ per group). Color images available online at www.liebertpub.com/tea

Table 1. Antibodies for Immunohistochemistry

	Dilution	*Supplier*
Primary antibodies		
Rb anti-GFP	1:300–500	Molecular Probes
G anti-OCN	1:100	Santa Cruz
SH anti-E11	1:100	Developmental Studies Hybridoma Bank
G anti-SDF-1 (C19)	1:400	Santa Cruz
Secondary antibodies		
FITC-conjugated G anti-Rb	1:200	Jackson ImmunoResearch
Cy3-conjugated D anti-G	1:200	Jackson ImmunoResearch
Cy3-conjugated G anti-SH	1:200	Jackson ImmunoResearch
Biotin-conjugated D anti G	1:200	Vector Laboratories
Reagents		
HRP-conjugated anti-Rb	1:400	Jackson ImmunoResearch
FITC-conjugated tyramide	1:800	Perkin Elmer
Biotin-conjugated tyramide	1:400	Perkin Elmer

D, donkey; G, goat; HRP, horseradish peroxidase; OCN, osteocalcin; Rb, rabbit; SDF-1, stromal cell-derived factor-1; SH, syrian hamster.

incubated with the appropriate fluorophore-conjugated secondary antibody (Table 1) for 2 h at room temperature in a humidifying chamber. Co-staining for GFP and SDF-1 was performed using the TSA Plus Fluorescein Kit (Table 1; Perkin Elmer) according to the manufacturer's recommendation. Sections were cover-slipped with Vectashield mounting medium (Vector Laboratories, Inc.) containing 4′,6-diamidino-2-phenylindole (DAPI) nuclear stain. Differential interference contrast (DIC) and fluorescence microscopy images were captured using a Carl Zeiss microscope with AxioVision Image Analysis software v4.7.1.0 (Carl Zeiss).

SDF-1α and SDF-1β enzyme-linked immunosorbent assay

SDF-1 splice variant-specific enzyme-linked immunosorbent assay (ELISAs; R&D Systems) of whole BM cells and BM interstitial fluids were performed as described previously.[37] Briefly, whole BM cell lysates were prepared in Complete Lysis-M EDTA-free buffer containing protease inhibitors (Roche Diagnostics). The anti-SDF-1 capture antibody (R&D Systems) in sodium bicarbonate buffer pH 9.4 was bound to MaxiSorp™ 96-well plates (Nunc, Thermo Fisher Scientific) overnight. Plates were blocked for 2 h with 1% BSA in PBS. Murine SDF-1α or SDF-1β (PeproTech) standards and samples (1:2 diluted) were incubated for 2 h prior to incubating with the biotinylated anti-SDF-1α and anti-SDF-1β detection antibody (2 h; R&D Systems), respectively. Streptavidin-horseradish peroxidase (R&D Systems) was incubated for 20 min followed by the substrate reagent (R&D Systems) for 20 min. Sulfuric acid (2 N) was added to stop the enzymatic color reaction and absorbance was read at 450 nm. SDF-1α and SDF-1β protein expression was calculated using standard curves and normalized to total protein, which was quantified using the EZQ® Protein Quantitation Kit (Invitrogen).

Dipeptidyl peptidase IV activity assay

Activity levels of dipeptidyl peptidase IV (DPPIV) were analyzed in undiluted BM interstitial fluids using a commercial fluorometric assay kit (H-Gly-Pro-AMC; Ex: 360 nm/Em: 465 nm at 30 min) (Enzo Life Sciences) according to the manufacturer's recommendation.

Transwell migration assay

Migration assays using BMSCs and BM interstitial fluids were performed according to a modified protocol described previously.[37] Briefly, BMSCs were transferred to phenol red-free DMEM supplemented with 1% FBS overnight. As a control, cells were pretreated with AMD3100 (1,1′-[1,4-phenylenebis(methylene)]-bis-1,4,8,11-tetraazacyclotetradecane octahydrochloride; Tocris Bioscience) at 400 μM for 4 h to competitively antagonize CXCR4 signaling in migratory BMSCs. The next day, BMSCs were lifted with trypsin/EDTA and resuspended at a density of 4.0×10^5 cells/mL in low serum DMEM. Fifty microliters of the BMSC suspension were added to the upper wells of a Transwell® 96-well system (8-μm pore size; Corning®, Thermo Fisher Scientific). As a source of chemoattractant, 150 μL of the BM interstitial fluids were added to the lower wells of the Transwell plate and BMSCs were incubated for 6 h at 37°C to allow cell migration across the porous membrane. Murine SDF-1α (100 ng/mL; PeproTech) was used as a positive control while low serum DMEM served as a negative/blank control. Migratory BMSCs at the bottom of the Transwell plate and adherent to the lower surface of the membrane were detached with trypsin/EDTA and lysed. Total DNA in the cell lysates was stained with CyQuant® GR Dye (Molecular Probes®, Thermo Fisher Scientific) and fluorescence was read at Ex: 485 nm/Em: 535 nm.

Quantitative reverse transcription–polymerase chain reaction

Quantitative reverse transcription–polymerase chain reaction (qRT-PCR) analysis of whole BM cells was performed as described previously.[37] Briefly, whole BM cells were lysed in TRIzol® reagent (Invitrogen) for RNA isolation and subsequent cDNA synthesis (iScript™ kit; Bio-Rad). One hundred nanograms of cDNA were amplified in duplicates in each 40-cycle reaction using an iCycler™ (Bio-Rad) with annealing temperature set at 60°C, ABsolute™ QPCR SYBR® Green Fluorescein Mix (ABgene, Thermo Fisher Scientific), and custom-designed qRT-PCR primers (Table 2; Thermo Fisher Scientific). A melt curve was used to assess the purity of amplification products. mRNA levels were normalized to β-Actin and gene expression was calculated as fold change using the comparative C_T method.

Statistical analysis

All data are expressed as mean ± SD. Bone morphometric parameters percent bone volume (BV/TV), BMD (trabecular bone), and trabecular number (Tb.N), thickness (Tb.Th) and

Table 2. Oligonucleotide Primer Sequences for Quantitative Reverse Transcription–Polymerase Chain Reaction

		Sequence (5′-3′)	*Product size*	*Accession number*
Gene				
SDF-1α	Fwd	GTGAGAACATGCCTAGATTTACCC	105	NM_021704
	Rev	ATAGGACTCAGGGACAATTACCAA		
SDF-1β	Fwd	GCTGAAGAACAACAACAGACAAGT	98	NM_013655
	Rev	CTCACATCTTGAGCCTCTTGTTTA		
DPPIV	Fwd	CCATTTTCTTGGAGAACAGTACCT	101	NM_010074
	Rev	CCATTGCTTCACGTAGTTGTATTC		
Neutrophil elastase	Fwd	CACTCGACAGACCTTCTCTGTG	85	NM_015779
	Rev	CTGGATAATCACAATGTCGTTCAG		
MMP-2	Fwd	GAAAAGATTGACGCTGTGTATGAG	105	NM_008610
	Rev	GTATCCTCGCTCCAGAGTACTAGC		
Cathepsin G	Fwd	CTACATGGCATTTCTTCTGATCC	120	NM_007800
	Rev	GTAACATTTATGGAGCTTCCCAAG		
Carboxypeptidase M	Fwd	AGAACCAACAAGCTTGGAGAATAC	109	NM_027468
	Rev	CTGGAATAGTAAGCTTCGTGAGGT		
Carboxypeptidase N	Fwd	GGTATCTGGTTGGTAGGAACAATG	96	AB021969
	Rev	CACCGTTCTTGGAGTTGTAGTAGA		
Housekeeping				
β-actin	Fwd	TGACAGACTACCTCATGAAGATCC	103	NM_007393
	Rev	ACATAGCACAGCTTCTCTTTGATG		

DPPIV, dipeptidyl peptidase IV; MMP-2, matrix metalloproteinase-2.

separation (Tb.Sp) were analyzed using a two-way repeated measures analysis of variance (RMANOVA). The model included treatment (TRT) (TRT: 1.32×10^5, 1.32×10^6, 6.60×10^6, or 1.32×10^7 cells/mL) as the fixed effect, BMSC transplantation (BMSC: no vs. yes) as the within animal repeated random effect, and the interaction between TRT and BMSC in both irradiated and nonirradiated conditions. A significant interaction effect would infer that the TRTs had a different effect on the outcome dependent on the presence or absence of BMSCs. The bone histomorphometric parameter BV/TV was analyzed in both irradiated and nonirradiated conditions using the nonparametric Spearman's rank correlation followed by the unpaired Student's *t* test. The unpaired Student's *t* test and one-way ANOVA were employed for BM interstitial fluid and BM cell analyses. A Tukey's *post hoc* test was used to test for significant effects. The significance level was set at alpha = 0.05 and SAS© v9.3 (SAS Institute, Inc.) was used for all analyses.

Results

BMSC engraftment and new bone formation

First, we investigated the effect of TBI on BMSC engraftment and new bone formation compared to nonirradiated controls employing *ex vivo* μCT. Representative 3D reconstructions at 4 weeks post-transplantation are depicted in Supplementary Figure S2. Quantitative analyses of bone morphometric parameters in the proximal tibiae using an ROI starting immediately beyond the epiphyseal plate and extending 2-mm distally by transaxial tracing revealed no apparent differences between vehicle and BMSC-transplanted tibiae in nonirradiated animals (Fig. 3A–E). In contrast, significantly increased percent bone volume (BV/TV, 0.6–4.1-fold, $p<0.0001$), trabecular number (Tb.N, 0.7–2.3-fold, $p<0.0001$), trabecular thickness (Tb.Th, 0.8–1.9-fold, $p<0.0001$), and BMD ([trabecular bone], 0.8–1.9-fold, $p<0.0001$) were found between vehicle and BMSC-transplanted tibiae in irradiated animals (Fig. 3F–H, J) with significant interactions ($p<0.0001$), dependent on the cell dose used. Trabecular separation (Tb.Sp) was significantly decreased (1.2–0.5-fold, $p<0.0001$) in BMSC-transplanted tibiae compared to controls (Fig. 3I) with significant interaction ($p=0.0003$). No differences were found between irradiated and nonirradiated vehicle controls across all bone morphometric parameters (Fig. 3A–J). Collectively, our findings suggest that TBI is permissive for BMSC-mediated new bone formation in a dose-dependent order.

Histology and bone histomorphometry

Qualitative histologic analysis mirrored the 3D microstructural bone evaluation and revealed the presence of mostly red marrow in the proximal head with no apparent differences in trabecular bone between vehicle and BMSC-transplanted tibiae in nonirradiated groups, irrespective of the cell dose used (Fig. 4A–E). In contrast, a dose-dependent increase in new bone formation was observed in tibiae transplanted with BMSCs relative to vehicle controls in irradiated animals, as evidenced by a greater amount of trabecular bone with predominantly white (fatty) marrow at lower cell doses and mostly red marrow at higher cell doses (Fig. 4F–J). This was confirmed by quantitative 2D bone histomorphometry. Percent bone volume (BV/TV) analysis revealed no differences between vehicle and BMSC-transplanted tibiae in nonirradiated animals (Fig. 2E). In contrast, significantly increased BV/TV (1.3–4.1-fold, $p<0.01$) was found between vehicle and BMSC-transplanted tibiae in irradiated animals, dependent on the cell dose used (Fig. 2F), thereby confirming the μCT data with significant correlation between methodologies (Spearman's rank correlation coefficient $r=0.85$, $p<0.0001$).

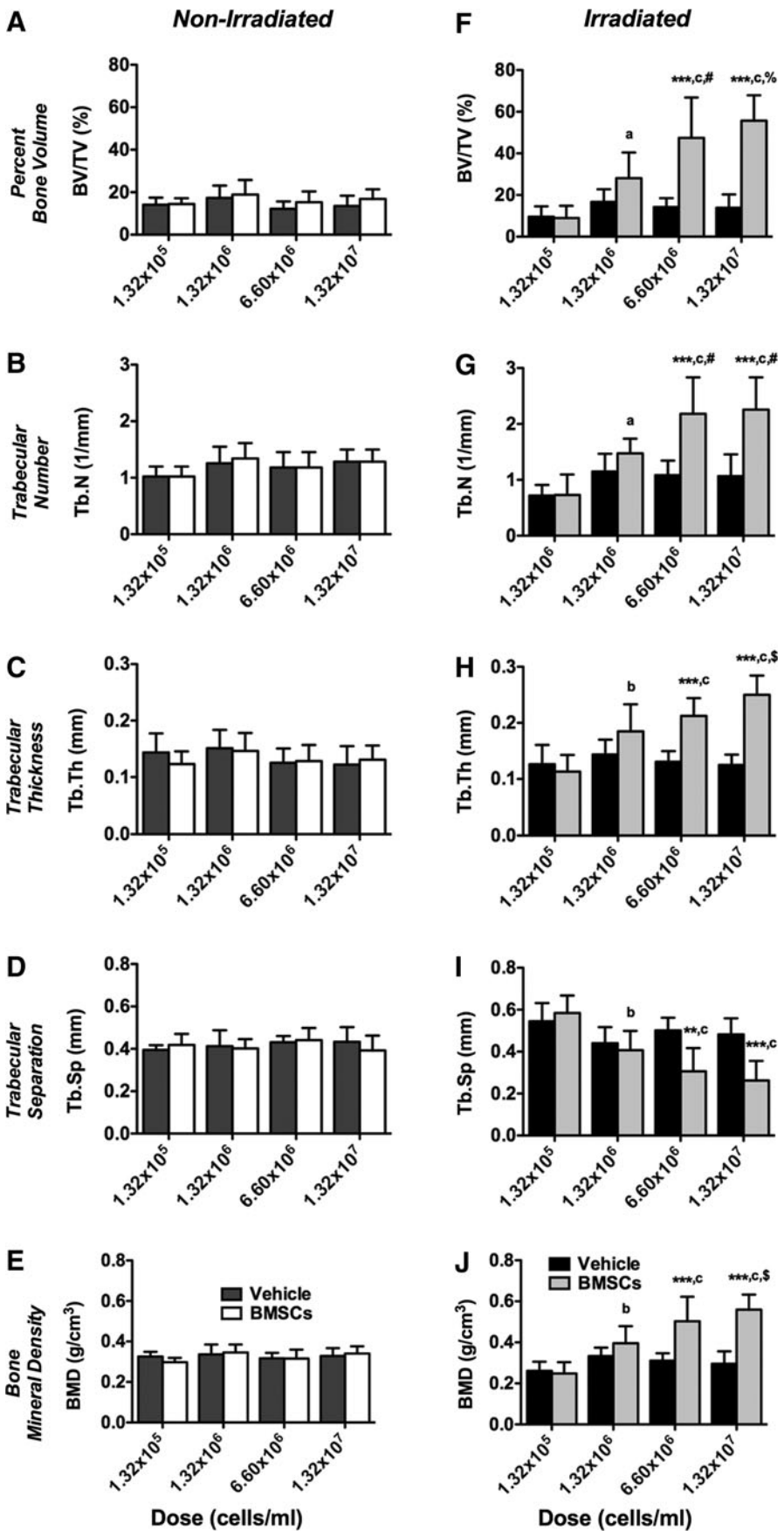

FIG. 3. Total body irradiation (TBI) significantly increases 3D bone morphometric parameters following bone marrow-derived mesenchymal stem/stromal cell (BMSC) transplantation in a cell dose-dependent fashion. Three-dimensional bone morphometric parameters of the proximal tibia marrow space 4 weeks post-transplantation (ROI: starting immediately beyond the epiphyseal plate and extending 2 mm distally by transaxial tracing for 135 cuts). **(A–E)** Nonirradiated and **(F–J)** irradiated animals. **(A, F)** Percent bone volume (BV/TV), **(B, G)** trabecular number (Tb.N), **(C, H)** trabecular thickness (Tb.Th), **(D, I)** trabecular separation (Tb.SP), and **(E, J)** bone mineral density (BMD; trabecular bone). Vehicle- and BMSC-transplanted tibiae at 1.32×10^5 (1%), 1.32×10^6 (10%), 6.60×10^6 (50%), or 1.32×10^7 cells/mL (100%) (***$p<0.001$ BMSC-transplanted vs. vehicle controls; [a]$p<0.05$, [b]$p<0.01$, [c]$p<0.0001$ 1.32×10^5 cells/mL vs. higher doses; [#]$p<0.05$, [$]$p<0.01$, [%]$p<0.0001$ 1.32×10^6 cells/mL vs. higher doses, $n=7$ animals per group).

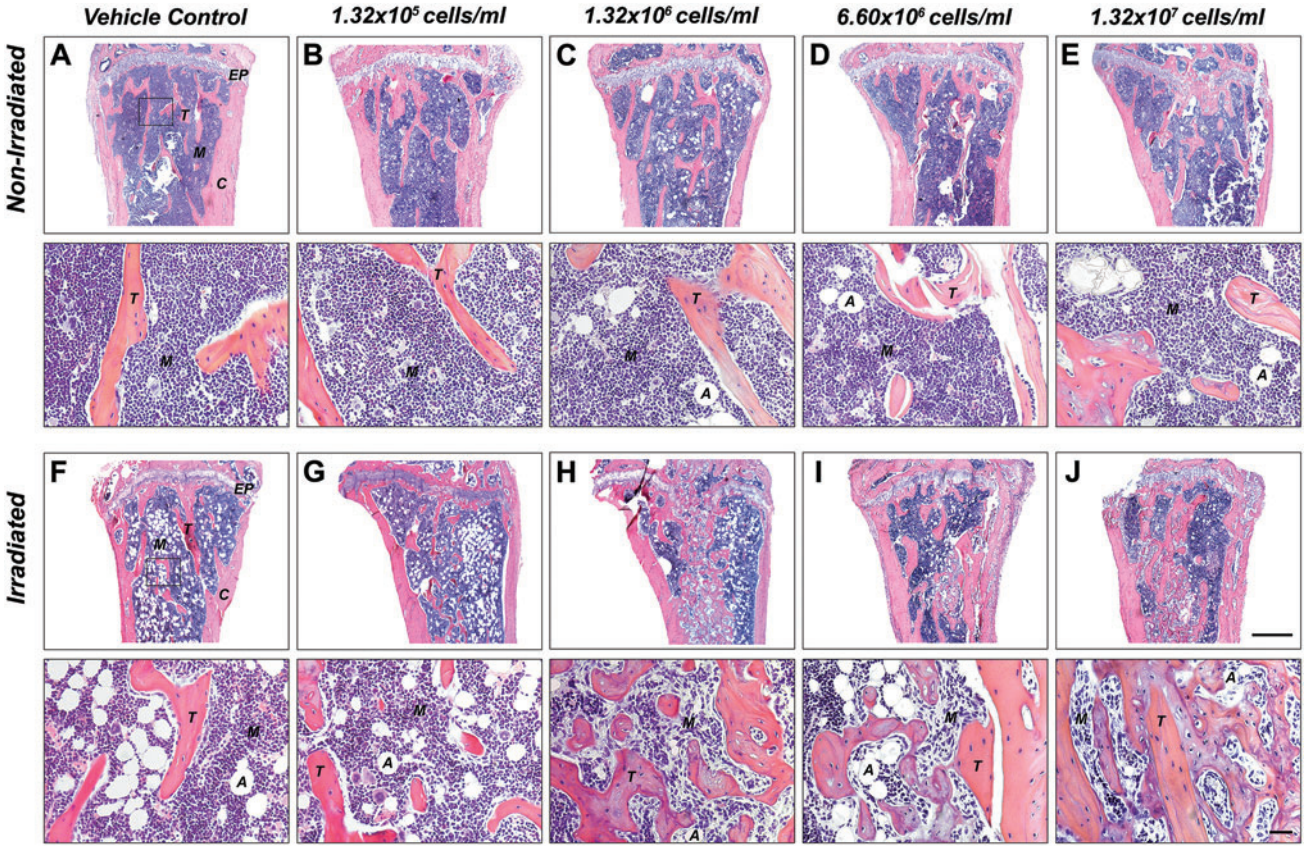

FIG. 4. TBI increases new bone formation in a cell dose-dependent fashion. Representative hematoxylin and eosin (H&E)-stained sections of the proximal tibia marrow space 4 weeks post-transplantation (ROI: starting immediately beyond the epiphyseal plate and extending 2 mm distally). **(A–E)** Nonirradiated and **(F–J)** irradiated animals. **(A, F)** Vehicle-transplanted (right) tibiae and BMSC-transplanted (left) tibiae at **(B, G)** 1.32×10^5 (1%), **(C, H)** 1.32×10^6 (10%), **(D, I)** 6.60×10^6 (50%), or **(E, J)** 1.32×10^7 cells/mL (100%) (EP: epiphyseal plate, M: marrow, T: trabecular bone, A: adipose tissue, C: cortical bone, 2.5×, scale bar 500 μm, 20×, scale bar 20 μm, $n=7$ animals per group). Color images available online at www.liebertpub.com/tea

Immunohistochemistry

Immunohistochemistry using a combined DIC/fluorescence microscopy approach showed virtually no GFP signal in the marrow space of nonirradiated BMSC-transplanted tibiae, comparable to vehicle controls (Fig. 5A–E). In contrast, a dose-dependent increase in the number of GFP-positive cells was observed, predominantly in the marrow space and lining trabecular structures contributing to the endosteum. In irradiation-preconditioned animals GFP-positive cells were found embedded in the trabecular bone matrix as osteocytes; however, the majority of the adjacent trabecular osteocytes were non-GFP expressing suggesting they were derived from endogenous progenitor cells. This implies that both the transplanted and endogenous BMSCs survived, engrafted, and contributed to new bone formation during the 4-week healing period following myeloablative injury (Fig. 5F–J). Qualitative fluorescence double-labeling studies revealed prominent expression levels of SDF-1 in conjunction with GFP following TBI (Fig. 6B1, 2), whereas overall limited SDF-1 expression was evident in nonirradiated BMSC-transplanted tibiae (Fig. 6A1, 2). Osteocalcin-positive osteoblasts exhibiting the characteristic cuboidal cell morphology were found lining the surface of trabecular structures with a subset co-expressing GFP indicative of their donor origin (Supplementary Fig. S3A1, 2). Maturing osteocytes embedded in the bone matrix, some of them also co-expressing GFP and the specific osteocyte marker E11, suggested that only a small fraction of the new bone was a result of direct osteogenic contributions from the transplanted BMSCs (Supplementary Fig. S3B1, 2).

BM interstitial fluid analyses

Next, we analyzed the BM microenvironment, specifically the BM interstitial fluid, extracted with PBS as the BM supernatant, and whole BM cells harvested from nonirradiated and irradiated animals. Using custom ELISAs, which employ splice variant specific detection antibodies, we found that normalized BM supernatant SDF-1α and SDF-1β protein levels were comparable between groups (Fig. 7A, B). These unexpected findings prompted the investigation of the DPPIV protease activity levels in the BM interstitial fluid, as DPPIV has been implicated in cleaving SDF-1 splice variants, which can cause impaired CXCR4 receptor activation. DPPIV activity was significantly enhanced ($p<0.05$) in TBI samples versus nonirradiated controls (Fig. 7C). Furthermore, using a Transwell bioassay, we showed that the chemotactic migration of BMSCs to BM supernatants of nonirradiated controls was significantly greater ($p<0.01$) compared with irradiated samples (Fig. 7D). This migratory effect toward nonirradiated

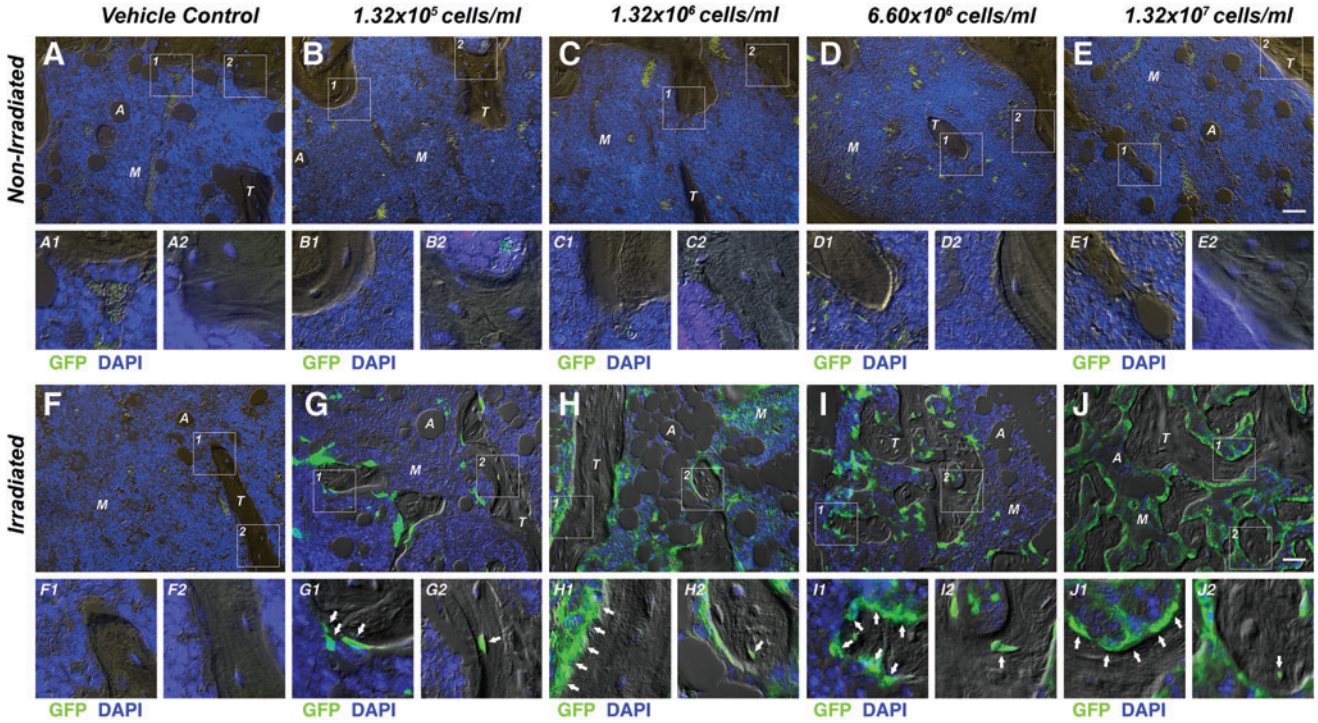

FIG. 5. TBI permits BMSC engraftment and new bone formation in a cell dose-dependent fashion. Representative combined differential interference contrast/fluorescence micrographs of the proximal tibia marrow space 4 weeks post-transplantation. **(A–E)** Nonirradiated and **(F–J)** irradiated animals. **(A, F)** Vehicle-transplanted (right) tibiae and BMSC-transplanted (left) tibiae at **(B, G)** 1.32×10^5 (1%), **(C, H)** 1.32×10^6 (10%), **(D, I)** 6.60×10^6 (50%), or **(E, J)** 1.32×10^7 cells/mL (100%). **(A–J1, 2)** GFP-positive cells lining trabecular structures and embedded in the bone matrix (arrows) (M: marrow, T: trabecular bone, A: adipose tissue, 20×, scale bar 20 μm, GFP = green, 4′,6-diamidino-2-phenylindole [DAPI] = blue, $n = 7$ animals per group). Color images available online at www.liebertpub.com/tea

BM supernatant was attenuated with AMD3100 (specific CXCR4 antagonist) pretreatment while no changes were observed in TBI samples (Fig. 7D), suggesting that the SDF-1α and SDF-1β secreted into the BM interstitial fluid is rendered biologically inactive at the observed time point 4 weeks post-transplantation.

BM cell analyses

In an effort to clarify the state of SDF-1 splice variants, we next analyzed transcript and protein levels in BM cells of irradiated and nonirradiated animals. Both SDF-1α and SDF-1β transcript levels in whole BM cells harvested from TBI

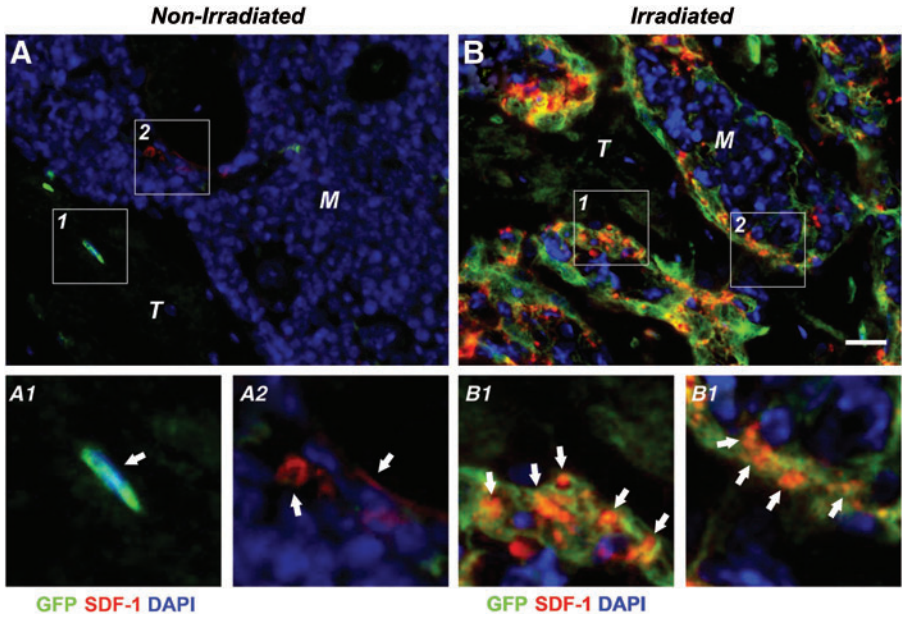

FIG. 6. Stromal cell-derived factor-1 (SDF-1) expression in irradiation-preconditioned animals is generally co-localized with transplanted BMSCs. Representative fluorescence micrographs of the proximal tibia marrow space of BMSC-transplanted tibiae at 1.32×10^7 cells/mL (100%) 4 weeks post-transplantation. **(A)** Non-irradiated and **(B)** irradiated animals. **(A1, 2)** Few GFP-positive or SDF-1-positive cells (*arrows*) lining trabecular structures without apparent co-localization in nonirradiated tibiae. **(B1, 2)** Abundant GFP- and SDF-1-double positive cells (*arrows*) in irradiated tibiae (M: marrow, T: trabecular bone, 40×, scale bar 40 μm, GFP = green, SDF-1 = red, DAPI = blue, $n = 7$ animals per group). Color images available online at www.liebertpub.com/tea

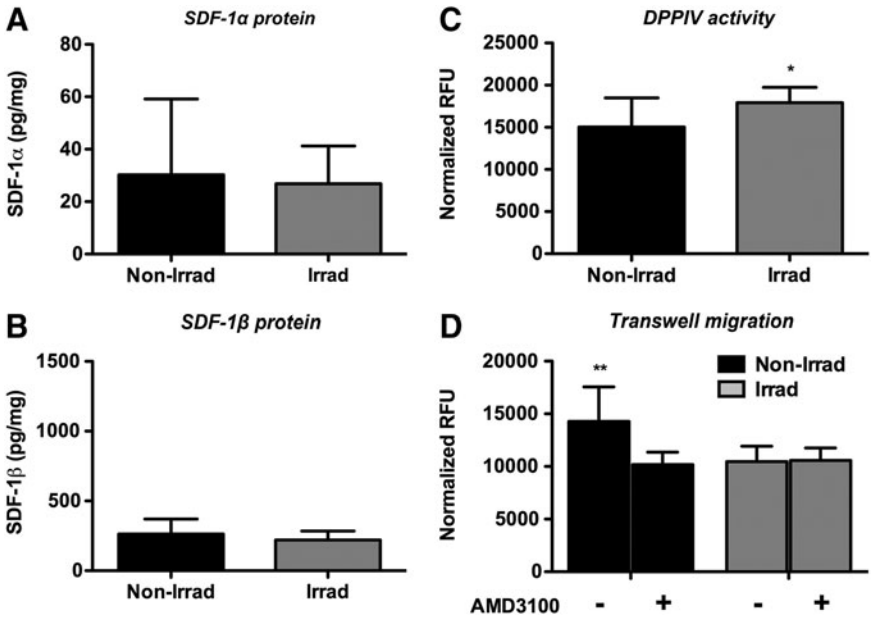

FIG. 7. TBI does not alter BM interstitial fluid SDF-1α and SDF-1β protein levels, but significantly enhances the dipeptidyl peptidase IV (DPPIV) activity and reduces the bioactivity at the 4-week end point. **(A, B)** Normalized SDF-1α and SDF-1β protein levels (n.s.). **(C)** Normalized DPPIV activity ($*p < 0.05$). **(D)** Normalized chemotactic migration of CXC chemokine receptor 4 (CXCR4)-expressing parental BMSCs ± CXCR4 receptor antagonist AMD3100 ($**p < 0.01$, $n = 7$ animals per group).

animals were significantly higher ($p < 0.05$, $p < 0.01$) compared with nonirradiated controls (Fig. 8A, B). SDF-1α and SDF-1β protein analyses showed a similar pattern, confirming the mRNA data (Fig. 8C, D). Subsequent transcript analysis of proteases implicated in splice variant-independent N-terminal cleavage of SDF-1 revealed significantly higher levels DPPIV ($p < 0.01$), neutrophil elastase ($p < 0.0001$), matrix metalloproteinase-2 (MMP-2, $p < 0.0001$), and cathepsin G ($p < 0.0001$) in irradiated samples versus nonirradiated controls (Fig. 9A–D). Interestingly, of the two proteases reported to cleave the C-terminus of SDF-1 in a splice variant-dependent fashion, only carboxypeptidase M (CPM) was found to be significantly upregulated ($p < 0.0001$) in irradiated BM cells while carboxypeptidase N (CPN) mRNA levels were comparable between groups (Fig. 9E, F).

Discussion

The aim of the present study was to investigate BMSC engraftment and new bone formation in a mouse model of local cell therapy, and the potential role of the chemokine SDF-1 in cell engraftment and subsequent bone formation. We tested the hypothesis that transplanted BMSCs induce osteogenesis in a dose-dependent manner, which is enhanced by TBI. Our data show that irradiation preconditioning is permissive for BMSC engraftment following direct tibial

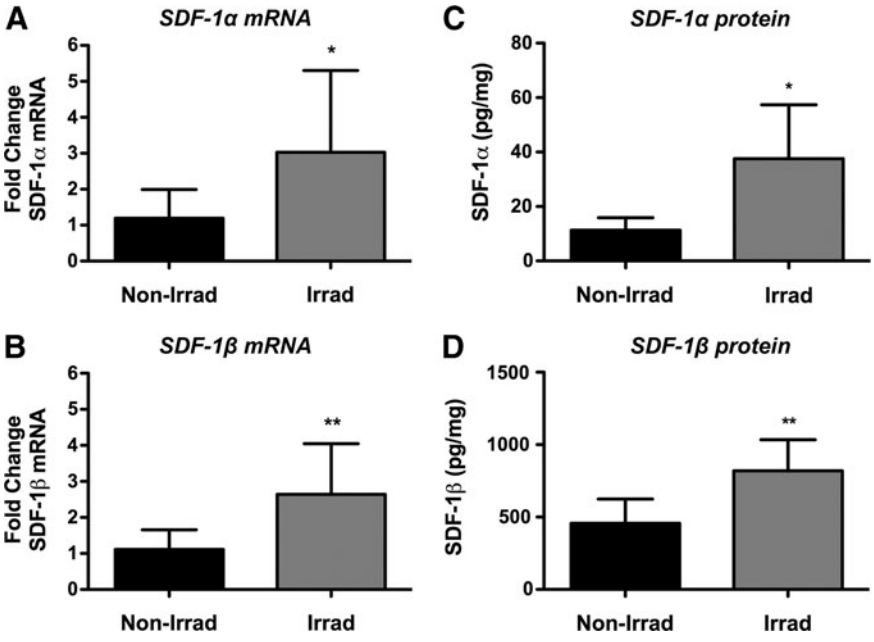

FIG. 8. TBI significantly upregulates whole BM cell SDF-1α and SDF-1β transcript and protein levels at the 4-week end point. **(A, B)** Normalized SDF-1α and SDF-1β mRNA levels ($*p < 0.05$, $**p < 0.01$). **(C, D)** Normalized SDF-1α and SDF-1β protein levels ($*p < 0.05$, $**p < 0.01$, $n = 7$ animals per group).

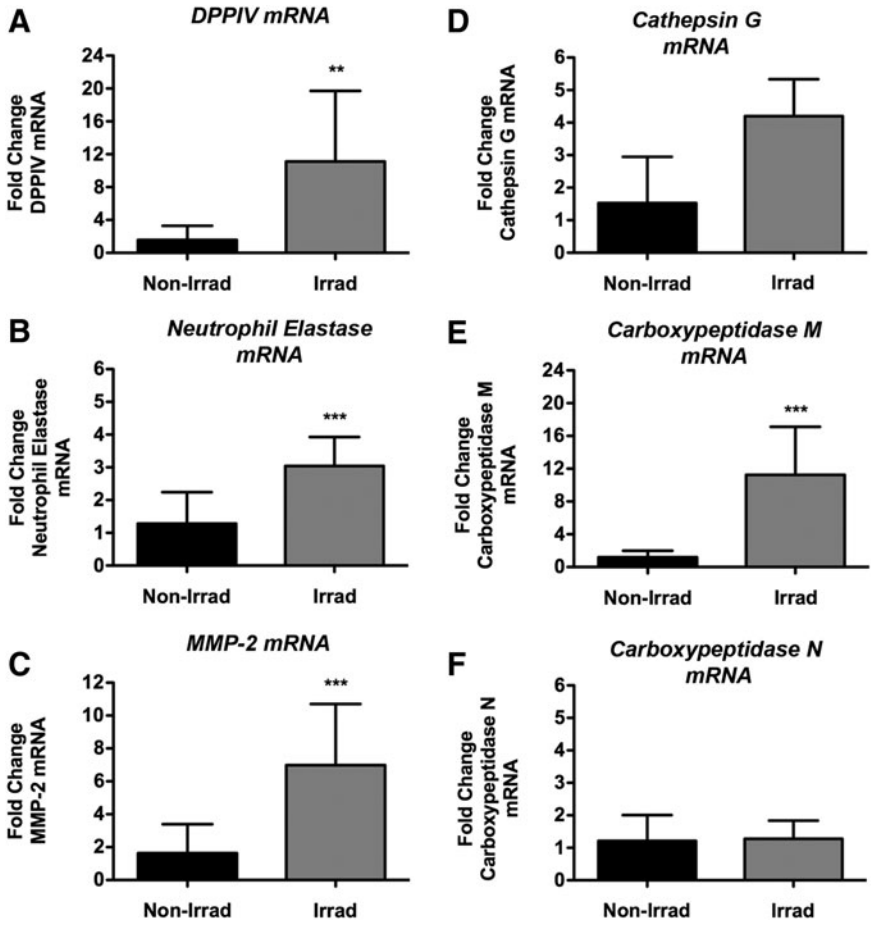

FIG. 9. TBI significantly upregulates whole BM cell transcript levels of SDF-1-cleaving proteases at the 4-week end point. Normalized mRNA levels of **(A)** DPPIV (**$p < 0.01$), **(B)** neutrophil elastase (***$p < 0.001$), **(C)** matrix metalloproteinase-2 (MMP-2) (***$p < 0.001$), **(D)** cathepsin G, **(E)** carboxypeptidase M (***$p < 0.001$), and **(F)** carboxypeptidase N (n.s., $n = 7$ animals per group).

transplantation. BMSCs contributed to new bone formation through both direct and indirect effects dependent on the cell dose used. Processing of SDF-1 splice variants in response to irradiation correlated with increased DPPIV activity levels and decreased bioactivity in the BM interstitial fluid 4 weeks post-transplantation, suggesting tightly regulated spatial chemokine activity.

Conditioning by radiation is widely used in preclinical and clinical protocols to ensure successful whole BM or BMSC transplantation.[15–18] This pretreatment creates space within the BM microenvironment by eliminating host stem cell populations and can also reduce the load of malignant cells in the diseased BM.[19] Compelling evidence suggests that SDF-1 is quickly upregulated in the BM in response to irradiation ($\sim$2 days), outlining the optimal time window for transplantation studies[19,53–56]; however, details of the SDF-1 expression levels over the course of a month-long healing interval remain largely unknown. It has been postulated that the increase in SDF-1 expression during injury situations is part of the host defense mechanism counteracting the effects of DNA-damaging regimens, which often result in cell death and anemia.[57,58] SDF-1 can increase the repopulation of the BM niche site following myeloablative injury by promoting the survival and proliferation of transplanted BM stem cells, including hematopoietic stem cells and BMSCs, in addition to enhancing the homing of macrophages, which aid in clearing apoptotic host cells from the irradiated BM.[16,19,46,48] By the same token, SDF-1 is also known to affect migration patterns of both injected and host BMSCs as well as circulating BM-derived osteoblast progenitors.[13,28,29] Lastly, indirect actions of implanted BMSCs, in particular secreting paracrine factors (such as SDF-1) to prolong the modulation of the host response, have been shown to be critical in bone tissue regeneration in addition to their direct osteogenic potential.[20–22]

We hypothesize that BMSC engraftment occurs in the irradiated BM following direct injection into the BM, in part, because intra-medullary injection permits large numbers of BMSCs to come into close physical contact with BMSC niche site cells that have been induced to express very high levels of SDF-1 on their surface, or in a narrow gradient near their surface. At the same time, the upregulation of SDF-1-degrading proteases significantly reduces secreted bioactive soluble SDF-1 in the BM interstitial fluid, consequently with reduced ability to support CXCR4 driven BMSC migration. What has come to light recently is that at very high concentrations SDF-1 switches the signaling pathway for CXCR4 (''biased agonism''), possibly by forming dimers,[59,60] from G-protein-coupled to β-arrestin mediated pathways.[59,61] When that switch occurs, one consequence is direct inhibition of cell migration, in effect retaining cells in place.[59,61] This switch inhibits actin reorganization via Rho GTPase regulation, and G-protein pathway mediated Ca^{2+} flux.[59,61] Our group has observed a similar trend of inhibited BMSC Transwell migration in response to very high concentrations of both SDF-1α and

SDF-1β (unpublished data). Therefore, we hypothesize that following irradiation the level of SDF-1 on, or near, the niche cell surface is high enough to induce the CXCR4 signaling biased agonism switch and retain the injected BMSCs that come into close approximation, permitting their engraftment and subsequent osteogenic influence on the BM microenvironment. In contrast, BMSC injection into nonirradiated BM see lower levels of SDF-1 on, or near, the surface of niche cells, below that required for the biased agonism switch. There is bioactive SDF-1 in the interstitial fluid permitting BMSC migration and allowing BMSCs to exit the BM without enhancing local bone formation.

Hence, we first investigated the effect of TBI on cell engraftment and BMSC-mediated new bone formation. The data indicated that, in our model, irradiation preconditioning is permissive for locally transplanted BMSCs to robustly engraft and contribute to new bone formation, as evidenced by 3D morphometric analysis of standard *ex vivo* μCT parameters.[49] Of note, no differences between irradiated and nonirradiated vehicle controls were found, suggesting that the commonly noted radiation-induced bone loss[62] was not detectable after 4 weeks in our model. This is most likely due to our rescuing transplantation of whole BM shortly after lethal irradiation, which reestablishes a significant portion of the BM progenitor and hematopoietic stem cell populations, and protects some of the surviving endogenous cells. In contrast, whole BM transplantation is often not used in sub-lethal irradiation models of bone injury.[62] Histology, 2D histomorphometry, and immunohistochemistry confirmed that new bone formation was limited to irradiation-preconditioned tibiae, regardless of the number of transplanted BMSCs. The low number of GFP-positive osteoblasts lining trabecular structures and making up the maturing osteocytes in new trabeculi suggested that the majority of the newly formed trabecular bone was derived from endogenous progenitor cells, or osteoblasts. Consistent with earlier reports was the presence of a greater density of marrow adipocytes within the proximal tibiae following irradiation compared with nonirradiated controls.[63] Importantly, using a combined DIC/fluorescence microscopy method, a large part of the marrow was found to contain GFP-positive cells within the marrow space and lining trabecular structures (as part of the endosteal lining cell layer or immediately adjacent to it) indicating that BMSCs survived, engrafted, and potentially secreted other stimulatory paracrine factors in addition to SDF-1, which was generally colocalized with GFP. In contrast, the marrow of nonirradiated controls showed very limited GFP signal suggesting that transplanted BMSCs did not engraft and/or were removed by the end of the 4-week healing interval. Taken together, it appears reasonable, that in a noninjury situation the presence and survival of supra-physiological levels of BMSCs in the BM is not supported. In contrast to hematopoietic stem cells, BMSCs do not readily engraft.

Splice variant-independent N-terminal cleavage of SDF-1α and SDF-1β, the two most abundant isoforms generated by alternative splicing,[64] which functionally inactivates the molecules, has been attributed to a number of different enzymes. Among these, DPPIV is catalytically active in serum and tissues and removes the first 2 amino acids.[30,31] Neutrophil elastase cleaves after the third amino acid[32], MMPs such as MMP-2 and 9 cut after the fourth amino acid[33], and cathepsin G cleaves after the fifth N-terminal amino acid in SDF-1.[34] Two proteases have been described to remove the C-terminal lysine of SDF-1α in a splice variant-dependent fashion, CPN[35] and CPM[36]; however, SDF-1β is protected from this proteolytic processing due to the presence of 4 additional C-terminal amino acids.[64] Several strategies have been successfully employed to modulate DPPIV activity in animal models. For example, small peptide molecules such as diprotin A (Ile-Pro-Ile) or Val-Pyr have been shown to effectively enhance stem cell engraftment, an effect likely due to inhibition of DPPIV truncation of both SDF-1 and nonchemokine growth factors.[48,65] This is the rationale for adopting DPP4 inhibition in our tibial transplantation model.

Analysis of the BM microenvironment suggested that whole BM cells from irradiation-preconditioned animals express greater amounts of SDF-1α and SDF-1β in comparison to cells from nonirradiated littermates. Hence, the lack of SDF-1 protein in the BM interstitial fluid is not due to suppression of transcription and translation, but rather a result of enhanced clearance in the interstitial fluid. Secreted SDF-1 splice variants were likely rendered inactive by extensive, and probably sequential, N-terminal proteolytic cleavage, beyond the functional inactivation by DPPIV, as shown by the loss of immunoreactive protein and failure to induce CXCR4 mediated Transwell migration of BMSCs. Supporting this notion and in agreement with a recent microarray-gene network study analyzing BM cells directly following TBI,[66] we found highly elevated transcript levels of the main proteases implicated in maintaining the SDF-1 protein homeostatic balance,[32–36] indirectly suggesting increased enzymatic activity. Previous work in our laboratory using whole BM cells and interstitial fluids harvested from normal femora and humeri has shown that the micro-injury due to saline injection does not alter the composition of the BM relative to normal uninjected tibiae at 4 weeks (unpublished data). Therefore, an extrapolation of the whole BM data from intact femora and humeri to injected tibiae in terms of the protease makeup appears feasible.

The BM interstitial fluid and BM cells are two distinct, spatially separated compartments of the BM niche site. Based on our findings, we speculate that SDF-1 protein levels in the BM interstitial fluid are rendered biologically inactive in irradiated mice approaching basal levels by 4 weeks through upregulation of the major SDF-1-cleaving proteases including DPPIV. The proteases are, in part, directly provided by the BM cells either secreted or bound to the cell surface. This suggests a control mechanism for maintaining the necessary homeostatic balance of active and inactive/antagonistic SDF-1 in the BM niche site in part balancing cell mobilization and homing. In contrast, BM cells in irradiated mice continue to express SDF-1 at higher than normal levels over 4 weeks, which may bind to CXCR4-expressing cells in an autocrine manner providing a positive feedback loop *in situ*. At the 4-week time point without a chemotactic gradient of active SDF-1 in the BM interstitial fluid, niche sites for CXCR4-expressing cells may be maintained by very restricted cell surface localization of SDF-1. With high proteolytic activity even the CXCR4 antagonist isoforms of cleaved SDF-1 would have short half-lives and be unlikely to act in a paracrine fashion. Any nonautocrine activity may require direct cell–cell interactions that limit

homing of cells from a distance, and migration or mobilization of cells within the niche. These findings have important implications for cancer treatment, which largely relies on radio- and chemotherapy protocols. Many malignant cells including leukemia and multiple myeloma cells, and breast and prostate cancer cells express CXCR4 and respond to SDF-1 gradients, which can result in BM infiltration and in some cases even bone lesions.[67–70] Of note, extensively cleaved SDF-1 isoforms are no longer able to bind and signal through (or block) CXCR4. This suggests that CXCR4-expressing cells in contact with cells expressing SDF-1 at high levels on their surface, or close to the surface, will be held in place due to the CXCR4 signaling biased agonism switch.[59,61] Further studies are warranted to investigate the risk of secondary malignancies in response to localized irradiation-induced BM production of SDF-1 as a consequence of this expression pattern, proteolytic processing, and potential subsequent changes in signaling.

Collectively, our findings suggest that both direct and indirect actions of the transplanted BMSCs are responsible for new bone formation upon local intramedullary transplantation in irradiation-preconditioned animals, with the latter appearing to play a significant role. Based on our findings, it appears likely that there are distinct differences between the broader BM microenvironment and the immediate BM cell surface portion of the niche site. Here, SDF-1 may play different, even opposing, roles with regard to autocrine and paracrine signaling beyond the direct cell surface microenvironment. These may change over the course of an injury response, in this case to irradiation. Our studies provide new evidence on how protease-mediated truncation of SDF-1 splice variants may be critical for spatial regulation of chemokine bioavailability and bioactivity; however, we can only speculate on the complex temporal expression patterns due to the single observation time point. Future studies aim to assess in greater detail the biological events following TBI that may regulate the success of subsequent BMSC transplantation in an effort to expand our understanding of the gradually changing ''biological fingerprint'' of the BM niche site over time, and ultimately to elucidate alternative approaches of preconditioning for BMSC transplantation without the need of employing irradiation or other translationally challenging approaches.

Acknowledgments

This publication is based upon work supported in part by the Department of Veterans Affairs, Veterans Health Administration, Office of Research and Development, Biomedical Laboratory Research and Development Program (VA Merit Award 104462, WDH) and the National Institutes of Health (NIA-AG036675-01, WDH). The contents of this publication do not represent the views of the Department of Veterans Affairs, or the United States Government. The authors appreciate the technical support of Donna Kumiski and Penny Roon, Georgia Regents University Histology Core Facility.

Disclosure Statement

The authors have no conflicts of interest.

References

1. Ito, H. Chemokines in mesenchymal stem cell therapy for bone repair: a novel concept of recruiting mesenchymal stem cells and the possible cell sources. Mod Rheumatol **21,** 113, 2011.
2. Sethe, S., Scutt, A., and Stolzing, A. Aging of mesenchymal stem cells. Ageing Res Rev **5,** 91, 2006.
3. Bonyadi, M., Waldman, S.D., Liu, D., Aubin, J.E., Grynpas, M.D., and Stanford, W.L. Mesenchymal progenitor self-renewal deficiency leads to age-dependent osteoporosis in Sca-1/Ly-6A null mice. Proc Natl Acad Sci U S A **100,** 5840, 2003.
4. Stolzing, A., Jones, E., McGonagle, D., and Scutt, A. Age-related changes in human bone marrow-derived mesenchymal stem cells: consequences for cell therapies. Mech Ageing Dev **129,** 163, 2008.
5. Caplan, A.I. Why are MSCs therapeutic? New data: new insight. J Pathol **217,** 318, 2009.
6. Korbling, M., and Estrov, Z. Adult stem cells for tissue repair—a new therapeutic concept? N Engl J Med **349,** 570, 2003.
7. Marcacci, M., Kon, E., Moukhachev, V., Lavroukov, A., Kutepov, S., Quarto, R., Mastrogiacomo, M., and Cancedda, R. Stem cells associated with macroporous bioceramics for long bone repair: 6- to 7-year outcome of a pilot clinical study. Tissue Eng **13,** 947, 2007.
8. Jones, E., and Yang, X. Mesenchymal stem cells and bone regeneration: current status. Injury **42,** 562, 2011.
9. Dominici, M., Pritchard, C., Garlits, J.E., Hofmann, T.J., Persons, D.A., and Horwitz, E.M. Hematopoietic cells and osteoblasts are derived from a common marrow progenitor after bone marrow transplantation. Proc Natl Acad Sci U S A **101,** 11761, 2004.
10. Horwitz, E.M., Gordon, P.L., Koo, W.K., Marx, J.C., Neel, M.D., McNall, R.Y., Muul, L., and Hofmann, T. Isolated allogeneic bone marrow-derived mesenchymal cells engraft and stimulate growth in children with osteogenesis imperfecta: implications for cell therapy of bone. Proc Natl Acad Sci U S A **99,** 8932, 2002.
11. Rieger, K., Marinets, O., Fietz, T., Korper, S., Sommer, D., Mucke, C., Reufi, B., Blau, W.I., Thiel, E., and Knauf, W.U. Mesenchymal stem cells remain of host origin even a long time after allogeneic peripheral blood stem cell or bone marrow transplantation. Exp Hematol **33,** 605, 2005.
12. Sarkar, D., Spencer, J.A., Phillips, J.A., Zhao, W., Schafer, S., Spelke, D.P., Mortensen, L.J., Ruiz, J.P., Vemula, P.K., Sridharan, R., Kumar, S., Karnik, R., Lin, C.P., and Karp, J.M. Engineered cell homing. Blood **118,** e184, 2011.
13. Granero-Molto, F., Weis, J.A., Miga, M.I., Landis, B., Myers, T.J., O'Rear, L., Longobardi, L., Jansen, E.D., Mortlock, D.P., and Spagnoli, A. Regenerative effects of transplanted mesenchymal stem cells in fracture healing. Stem Cells **27,** 1887, 2009.
14. Herberg, S., Shi, X., Johnson, M.H., Hamrick, M.W., Isales, C.M., and Hill, W.D. Stromal cell-derived factor-1 beta mediates cell survival through enhancing autophagy in bone marrow-derived mesenchymal stem cells. PLoS One **8,** e58207, 2013.
15. Francois, S., Bensidhoum, M., Mouiseddine, M., Mazurier, C., Allenet, B., Semont, A., Frick, J., Sache, A., Bouchet, S., Thierry, D., Gourmelon, P., Gorin, N.C., and Chapel, A. Local irradiation not only induces homing of human mesenchymal stem cells at exposed sites but promotes their widespread engraftment to multiple organs: a study of their

quantitative distribution after irradiation damage. Stem Cells **24,** 1020, 2006.
16. Wang, L., Liu, Y., Kalajzic, Z., Jiang, X., and Rowe, D.W. Heterogeneity of engrafted bone-lining cells after systemic and local transplantation. Blood **106,** 3650, 2005.
17. Mouiseddine, M., Francois, S., Semont, A., Sache, A., Allenet, B., Mathieu, N., Frick, J., Thierry, D., and Chapel, A. Human mesenchymal stem cells home specifically to radiation-injured tissues in a non-obese diabetes/severe combined immunodeficiency mouse model. Br J Radiol **80 Spec No 1,** S49, 2007.
18. Chapel, A., Bertho, J.M., Bensidhoum, M., Fouillard, L., Young, R.G., Frick, J., Demarquay, C., Cuvelier, F., Mathieu, E., Trompier, F., Dudoignon, N., Germain, C., Mazurier, C., Aigueperse, J., Borneman, J., Gorin, N.C., Gourmelon, P., and Thierry, D. Mesenchymal stem cells home to injured tissues when co-infused with hematopoietic cells to treat a radiation-induced multi-organ failure syndrome. J Gene Med **5,** 1028, 2003.
19. Ponomaryov, T., Peled, A., Petit, I., Taichman, R.S., Habler, L., Sandbank, J., Arenzana-Seisdedos, F., Magerus, A., Caruz, A., Fujii, N., Nagler, A., Lahav, M., Szyper-Kravitz, M., Zipori, D., and Lapidot, T. Induction of the chemokine stromal-derived factor-1 following DNA damage improves human stem cell function. J Clin Invest **106,** 1331, 2000.
20. Scotti, C., Tonnarelli, B., Papadimitropoulos, A., Scherberich, A., Schaeren, S., Schauerte, A., Lopez-Rios, J., Zeller, R., Barbero, A., and Martin, I. Recapitulation of endochondral bone formation using human adult mesenchymal stem cells as a paradigm for developmental engineering. Proc Natl Acad Sci U S A **107,** 7251, 2010.
21. Tortelli, F., Tasso, R., Loiacono, F., and Cancedda, R. The development of tissue-engineered bone of different origin through endochondral and intramembranous ossification following the implantation of mesenchymal stem cells and osteoblasts in a murine model. Biomaterials **31,** 242, 2010.
22. Caplan, A.I., and Dennis, J.E. Mesenchymal stem cells as trophic mediators. J Cell Biochem **98,** 1076, 2006.
23. Zlotnik, A., and Yoshie, O. Chemokines: a new classification system and their role in immunity. Immunity **12,** 121, 2000.
24. Bleul, C.C., Farzan, M., Choe, H., Parolin, C., Clark-Lewis, I., Sodroski, J., and Springer, T.A. The lymphocyte chemoattractant SDF-1 is a ligand for LESTR/fusin and blocks HIV-1 entry. Nature **382,** 829, 1996.
25. Feng, Y., Broder, C.C., Kennedy, P.E., and Berger, E.A. HIV-1 entry cofactor: functional cDNA cloning of a seven-transmembrane, G protein-coupled receptor. Science **272,** 872, 1996.
26. Heesen, M., Berman, M.A., Benson, J.D., Gerard, C., and Dorf, M.E. Cloning of the mouse fusin gene, homologue to a human HIV-1 co-factor. J Immunol **157,** 5455, 1996.
27. Kucia, M., Jankowski, K., Reca, R., Wysoczynski, M., Bandura, L., Allendorf, D.J., Zhang, J., Ratajczak, J., and Ratajczak, M.Z. CXCR4-SDF-1 signalling, locomotion, chemotaxis and adhesion. J Mol Histol **35,** 233, 2004.
28. Kitaori, T., Ito, H., Schwarz, E.M., Tsutsumi, R., Yoshitomi, H., Oishi, S., Nakano, M., Fujii, N., Nagasawa, T., and Nakamura, T. Stromal cell-derived factor 1/CXCR4 signaling is critical for the recruitment of mesenchymal stem cells to the fracture site during skeletal repair in a mouse model. Arthritis Rheum **60,** 813, 2009.
29. Otsuru, S., Tamai, K., Yamazaki, T., Yoshikawa, H., and Kaneda, Y. Circulating bone marrow-derived osteoblast progenitor cells are recruited to the bone-forming site by the CXCR4/stromal cell-derived factor-1 pathway. Stem Cells **26,** 223, 2008.
30. De La Luz Sierra, M., Yang, F., Narazaki, M., Salvucci, O., Davis, D., Yarchoan, R., Zhang, H.H., Fales, H., and Tosato, G. Differential processing of stromal-derived factor-1 alpha and stromal-derived factor-1beta explains functional diversity. Blood **103,** 2452, 2004.
31. Lambeir, A.M., Proost, P., Durinx, C., Bal, G., Senten, K., Augustyns, K., Scharpe, S., Van Damme, J., and De Meester, I. Kinetic investigation of chemokine truncation by CD26/dipeptidyl peptidase IV reveals a striking selectivity within the chemokine family. J Biol Chem **276,** 29839, 2001.
32. Valenzuela-Fernandez, A., Planchenault, T., Baleux, F., Staropoli, I., Le-Barillec, K., Leduc, D., Delaunay, T., Lazarini, F., Virelizier, J.L., Chignard, M., Pidard, D., and Arenzana-Seisdedos, F. Leukocyte elastase negatively regulates Stromal cell-derived factor-1 (SDF-1)/CXCR4 binding and functions by amino-terminal processing of SDF-1 and CXCR4. J Biol Chem **277,** 15677, 2002.
33. McQuibban, G.A., Butler, G.S., Gong, J.H., Bendall, L., Power, C., Clark-Lewis, I., and Overall, C.M. Matrix metalloproteinase activity inactivates the CXC chemokine stromal cell-derived factor-1. J Biol Chem **276,** 43503, 2001.
34. Delgado, M.B., Clark-Lewis, I., Loetscher, P., Langen, H., Thelen, M., Baggiolini, M., and Wolf, M. Rapid inactivation of stromal cell-derived factor-1 by cathepsin G associated with lymphocytes. Eur J Immunol **31,** 699, 2001.
35. Davis, D.A., Singer, K.E., De La Luz Sierra, M., Narazaki, M., Yang, F., Fales, H.M., Yarchoan, R., and Tosato, G. Identification of carboxypeptidase N as an enzyme responsible for C-terminal cleavage of stromal cell-derived factor-1alpha in the circulation. Blood **105,** 4561, 2005.
36. Marquez-Curtis, L., Jalili, A., Deiteren, K., Shirvaikar, N., Lambeir, A.M., and Janowska-Wieczorek, A. Carboxypeptidase M expressed by human bone marrow cells cleaves the C-terminal lysine of stromal cell-derived factor-1alpha: another player in hematopoietic stem/progenitor cell mobilization? Stem Cells **26,** 1211, 2008.
37. Herberg, S., Fulzele, S., Yang, N., Shi, X., Hess, M., Periyasamy-Thandavan, S., Hamrick, M.W., Isales, C.M., and Hill, W.D. Stromal cell-derived factor-1beta potentiates bone morphogenetic protein-2-stimulated osteoinduction of genetically engineered bone marrow-derived mesenchymal stem cells *in vitro*. Tissue Eng Part A **19,** 1, 2013.
38. Zhang, W., Ou, G., Hamrick, M., Hill, W., Borke, J., Wenger, K., Chutkan, N., Yu, J., Mi, Q.S., Isales, C.M., and Shi, X.M. Age-related changes in the osteogenic differentiation potential of mouse bone marrow stromal cells. J Bone Miner Res **23,** 1118, 2008.
39. Zhang, W., Yang, N., and Shi, X.M. Regulation of mesenchymal stem cell osteogenic differentiation by glucocorticoid-induced leucine zipper (GILZ). J Biol Chem **283,** 4723, 2008.
40. Gimble, J.M., Robinson, C.E., Wu, X., Kelly, K.A., Rodriguez, B.R., Kliewer, S.A., Lehmann, J.M., and Morris, D.C. Peroxisome proliferator-activated receptor-gamma activation by thiazolidinediones induces adipogenesis in bone marrow stromal cells. Mol Pharmacol **50,** 1087, 1996.

41. Peister, A., Mellad, J.A., Larson, B.L., Hall, B.M., Gibson, L.F., and Prockop, D.J. Adult stem cells from bone marrow (MSCs) isolated from different strains of inbred mice vary in surface epitopes, rates of proliferation, and differentiation potential. Blood **103,** 1662, 2004.
42. Tropel, P., Noel, D., Platet, N., Legrand, P., Benabid, A.L., and Berger, F. Isolation and characterisation of mesenchymal stem cells from adult mouse bone marrow. Exp Cell Res **295,** 395, 2004.
43. Down, J.D., Tarbell, N.J., Thames, H.D., and Mauch, P.M. Syngeneic and allogeneic bone marrow engraftment after total body irradiation: dependence on dose, dose rate, and fractionation. Blood **77,** 661, 1991.
44. Duran-Struuck, R., and Dysko, R.C. Principles of bone marrow transplantation (BMT): providing optimal veterinary and husbandry care to irradiated mice in BMT studies. J Am Assoc Lab Anim Sci **48,** 11, 2009.
45. Hanson, W.R., Fry, R.J., Sallese, A.R., Frischer, H., Ahmad, T., and Ainsworth, E.J. Comparison of intestine and bone marrow radiosensitivity of the BALB/c and the C57BL/6 mouse strains and their B6CF1 offspring. Radiat Res **110,** 340, 1987.
46. Yang, Y., Schumacher, A., Yang, Y., Liu, J., Shi, X., Hill, W.D., and Hu, T.C. Monitoring bone marrow-originated mesenchymal stem cell traffic to myocardial infarction sites using magnetic resonance imaging. Magn Reson Med **65,** 1430, 2011.
47. Day, R.M., Davis, T.A., Barshishat-Kupper, M., McCart, E.A., Tipton, A.J., and Landauer, M.R. Enhanced hematopoietic protection from radiation by the combination of genistein and captopril. Int Immunopharmacol **15,** 348, 2013.
48. Christopherson, K.W., 2nd, Hangoc, G., Mantel, C.R., and Broxmeyer, H.E. Modulation of hematopoietic stem cell homing and engraftment by CD26. Science **305,** 1000, 2004.
49. Bouxsein, M.L., Boyd, S.K., Christiansen, B.A., Guldberg, R.E., Jepsen, K.J., and Muller, R. Guidelines for assessment of bone microstructure in rodents using micro-computed tomography. J Bone Miner Res **25,** 1468, 2010.
50. Dempster, D.W., Compston, J.E., Drezner, M.K., Glorieux, F.H., Kanis, J.A., Malluche, H., Meunier, P.J., Ott, S.M., Recker, R.R., and Parfitt, A.M. Standardized nomenclature, symbols, and units for bone histomorphometry: a 2012 update of the report of the ASBMR Histomorphometry Nomenclature Committee. J Bone Miner Res **28,** 2, 2013.
51. Parfitt, A.M., Drezner, M.K., Glorieux, F.H., Kanis, J.A., Malluche, H., Meunier, P.J., Ott, S.M., and Recker, R.R. Bone histomorphometry: standardization of nomenclature, symbols, and units. Report of the ASBMR Histomorphometry Nomenclature Committee. J Bone Miner Res **2,** 595, 1987.
52. Egan, K.P., Brennan, T.A., and Pignolo, R.J. Bone histomorphometry using free and commonly available software. Histopathology **61,** 1168, 2012.
53. Thanik, V.D., Chang, C.C., Lerman, O.Z., Greives, M.R., Le, H., Warren, S.M., Schneider, R.J., Formenti, S.C., Saadeh, P.B., and Levine, J.P. Cutaneous low-dose radiation increases tissue vascularity through upregulation of angiogenic and vasculogenic pathways. J Vasc Res **47,** 472, 2010.
54. Dominici, M., Rasini, V., Bussolari, R., Chen, X., Hofmann, T.J., Spano, C., Bernabei, D., Veronesi, E., Bertoni, F., Paolucci, P., Conte, P., and Horwitz, E.M. Restoration and reversible expansion of the osteoblastic hematopoietic stem cell niche after marrow radioablation. Blood **114,** 2333, 2009.
55. Bastianutto, C., Mian, A., Symes, J., Mocanu, J., Alajez, N., Sleep, G., Shi, W., Keating, A., Crump, M., Gospodarowicz, M., Medin, J., Minden, M., and Liu, F.F. Local radiotherapy induces homing of hematopoietic stem cells to the irradiated bone marrow. Cancer Res **67,** 10112, 2007.
56. Zong, Z.W., Cheng, T.M., Su, Y.P., Ran, X.Z., Li, N., Ai, G.P., and Xu, H. Crucial role of SDF-1/CXCR4 interaction in the recruitment of transplanted dermal multipotent cells to sublethally irradiated bone marrow. J Radiat Res **47,** 287, 2006.
57. Lataillade, J.J., Clay, D., Dupuy, C., Rigal, S., Jasmin, C., Bourin, P., and Le Bousse-Kerdiles, M.C. Chemokine SDF-1 enhances circulating CD34(+) cell proliferation in synergy with cytokines: possible role in progenitor survival. Blood **95,** 756, 2000.
58. Grafte-Faure, S., Leveque, C., Ketata, E., Jean, P., Vasse, M., Soria, C., and Vannier, J.P. Recruitment of primitive peripheral blood cells: synergism of interleukin 12 with interleukin 6 and stromal cell-derived FACTOR-1. Cytokine **12,** 1, 2000.
59. Drury, L.J., Ziarek, J.J., Gravel, S., Veldkamp, C.T., Takekoshi, T., Hwang, S.T., Heveker, N., Volkman, B.F., and Dwinell, M.B. Monomeric and dimeric CXCL12 inhibit metastasis through distinct CXCR4 interactions and signaling pathways. Proc Natl Acad Sci U S A **108,** 17655, 2011.
60. Takekoshi, T., Ziarek, J.J., Volkman, B.F., and Hwang, S.T. A locked, dimeric CXCL12 variant effectively inhibits pulmonary metastasis of CXCR4-expressing melanoma cells due to enhanced serum stability. Mol Cancer Ther **11,** 2516, 2012.
61. Reiter, E., Ahn, S., Shukla, A.K., and Lefkowitz, R.J. Molecular mechanism of beta-arrestin-biased agonism at seven-transmembrane receptors. Annu Rev Pharmacol Toxicol **52,** 179, 2012.
62. Green, D.E., Adler, B.J., Chan, M.E., and Rubin, C.T. Devastation of adult stem cell pools by irradiation precedes collapse of trabecular bone quality and quantity. J Bone Miner Res **27,** 749, 2012.
63. Georgiou, K.R., Hui, S.K., and Xian, C.J. Regulatory pathways associated with bone loss and bone marrow adiposity caused by aging, chemotherapy, glucocorticoid therapy and radiotherapy. Am J Stem Cells **1,** 205, 2012.
64. Yu, L., Cecil, J., Peng, S.B., Schrementi, J., Kovacevic, S., Paul, D., Su, E.W., and Wang, J. Identification and expression of novel isoforms of human stromal cell-derived factor 1. Gene **374,** 174, 2006.
65. Broxmeyer, H.E. Enhancing engraftment of cord blood cells via insight into the biology of stem/progenitor cell function. Ann N Y Acad Sci **1266,** 151, 2012.
66. Zhang, J., Yang, Y., Wang, Y., Wang, Z., Yin, M., and Shen, X. Identification of hub genes related to the recovery phase of irradiation injury by microarray and integrated gene network analysis. PLoS One **6,** e24680, 2011.
67. Lalle, M., De Rosa, L., Marzetti, L., and Montuoro, A. Detection of breast cancer cells in the bone marrow or peripheral blood: methods and prognostic significance. Tumori **86,** 183, 2000.
68. Bradstock, K.F., Makrynikola, V., Bianchi, A., Shen, W., Hewson, J., and Gottlieb, D.J. Effects of the chemokine stromal cell-derived factor-1 on the migration and localization of precursor-B acute lymphoblastic leukemia cells within bone marrow stromal layers. Leukemia **14,** 882, 2000.

69. Koshiba, T., Hosotani, R., Miyamoto, Y., Ida, J., Tsuji, S., Nakajima, S., Kawaguchi, M., Kobayashi, H., Doi, R., Hori, T., Fujii, N., and Imamura, M. Expression of stromal cell-derived factor 1 and CXCR4 ligand receptor system in pancreatic cancer: a possible role for tumor progression. Clin Cancer Res **6,** 3530, 2000.
70. Mochizuki, H., Matsubara, A., Teishima, J., Mutaguchi, K., Yasumoto, H., Dahiya, R., Usui, T., and Kamiya, K. Interaction of ligand-receptor system between stromal-cell-derived factor-1 and CXC chemokine receptor 4 in human prostate cancer: a possible predictor of metastasis. Biochem Biophys Res Commun **320,** 656, 2004.

Address correspondence to:
William D. Hill, PhD
Department of Cellular Biology and Anatomy
Georgia Regents University
CB-1119, 1459 Laney Walker Boulevard
Augusta, GA 30912

E-mail: whill@gru.edu

Received: October 23, 2013
Accepted: May 28, 2014
Online Publication Date: October 17, 2014